Artificial Retardation of Barotropic Waves in Layered Ocean Models

TOMMY G. JENSEN

Department of Atmospheric Science, Colorado State University, Fort Collins, Colorado and International Research Centre for Computational Hydrodynamics, Danish Hydraulic Institute, Hørsholm, Denmark

(Manuscript received 1 May 1995, in final form 23 October 1995)

ABSTRACT

The effect of reducing the barotropic gravity wave speed in a layered ocean model in order to gain computational speed is explored. In theory the error in the propagation of baroclinic gravity waves typically is less than 3% for a reduction of the external gravity speed by one order of magnitude. This is confirmed in a numerical experiment. For baroclinic Rossby waves, the phase speed error is even less. The barotropic response is limited to the reduced radius of deformation. The method, which we will refer to as gravity wave retardation, is therefore applicable only for oceanic flows where the barotropic mode is of minor importance. It is demonstrated that the method gives very good results for the baroclinic flow of an equatorial jet, spinup of a midlatitude ocean and flow over a midoceanic ridge. The method can be considered as an alternative to multilayer reduced gravity models, and has the advantage that bottom topography can be included.

1. Introduction

For phenomena with timescales larger than a few days, external gravity waves do not contribute directly, but play a role in the oceanic adjustment to changes in external forcing. For basin and global-scale ocean models, the barotropic mode is often separated from the internal modes and solved separately because of the large phase speed associated with the gravity waves. For instance, in the Bryan–Cox and Semtner–Chervin type model, a rigid lid has traditionally been applied and an elliptic equation for the barotropic streamfunction or surface pressure has been solved (Bryan 1969; Smith et al. 1992). In a later version (Dukowicz and Smith 1994), an implicit formulation for the free surface elevation is used, which also requires solution of an elliptic equation.

In the Blumberg–Mellor model (Blumberg and Mellor 1987), the external mode is separated out and solved explicitly with a short time step. A similar method is used in the Miami isopycnal model (Bleck and Smith 1990) by Killworth et al. (1991) for their free surface version of the Bryan–Cox model and by Zhang and Endoh (1992) for their Pacific Ocean model. However, the coupling between the baroclinic mode and the subcycled barotropic mode is not trivial as reported by those investigators.

By selecting a reduced gravity model with a single active layer, Cushman-Roisin and O'Brien (1983) eliminated the barotropic mode entirely. By substituting the internal gravity wave speed in the momentum equation for the active layer with the analytical phase speed for a two-layer ocean, they were able to include effects of bottom topography on the baroclinic mode. However, an extension of their approach to the multilayer models is not straightforward.

In the models above, the barotropic mode is either eliminated in part (rigid lid) or entirely (reduced gravity models) or separated out and treated specially (free surface models). While separating the barotropic mode out in general requires decomposition onto vertical modes (e.g., solving a general eigenvalue problem, see Gill 1982, 159–162), a simple vertical average of the equations are most often used to approximate the barotropic mode. Because of this approximation, the remaining baroclinic equations may contain a small part of the fast mode, and the models may be weakly unstable unless sufficient diffusion is added.

The Naval Research Laboratory model (Wallcraft 1991) uses a semi-implicit formulation for all gravity waves, which requires normal-mode decomposition and solution of an elliptic equation for each vertical mode. The Hamburg isopycnal ocean model (Oberhuber 1993) is fully implicit and also requires matrix inversions.

In this paper, a method of reducing the external gravity wave speed is explored. This is very similar to the method of artificial compressibility used in computational hydrodynamics (Chorin 1967). The method used here works by reducing the slope of the sea surface in the momentum equation, which is equivalent to

Corresponding author address: Dr. Tommy G. Jensen, Department of Atmospheric Science, Colorado State University, Fort Collins, CO 80523.
E-mail: jensen@neptune.atmos.colostate.edu

reducing the constant of gravity for the surface waves. At a CHAMMP Science Team Meeting in 1994, John Anderson and Michael Tobis presented modeling results where the latter technique was used. Further details on their method are given by Tobis (1996).

Bryan (1984) presented a method of distorted physics for accelerated convergence toward steady state for ocean climate models. As in the method by Chorin (1967), only the time derivative is changed, so the steady solution (assuming that one exists) is the same for the modified equations as for the original equations. One consequence of that method is that wave speeds are strongly reduced for gravity waves as well as planetary waves, since it involves changing both the rate of rotation of the earth and the acceleration of gravity.

A method of reducing the magnitude of gravity alone has previously been applied to hydrodynamical models for homogeneous seas (Hearn and Hunter 1987) and in a modified form by Hunter (1990a,b). A similar approach is applied to a stratified ocean in this paper. The main advantages of the method presented here are that for layered models it is simple to use without a formal separation of external and internal modes, and that the internal (baroclinic) modes basically are unaffected.

2. The ocean model

The ocean model is that of Jensen (1991, 1993) modified to include finite depth. In this paper, we apply a rectangular coordinate system and choose $z = 0$ to be the surface of the ocean at rest. Define vertically integrated volume transport components U_j and V_j by

$$U_j = \int_{z_j}^{z_{j+1}} u dz \tag{1}$$

between two surfaces $z_j(x, y, t)$ and $z_{j+1}(x, y, t)$, with an equivalent expression for V_j. The thickness of the jth layer defined by this integration is $H_j = (z_{j+1} - z_j)$.

An ocean consisting of several layers of uniform density is shown in Fig. 1. We assume that all layers have a positive thickness everywhere. This implies that layers are not allowed to surface or merge, and that the bottom topography is always in the lowest layer. If the density of the jth layer is given by ρ_j, the zonal transport U_j for that layer becomes

$$\frac{\partial U_j}{\partial t} + \frac{\partial}{\partial x}\left(\frac{U_j^2}{H_j}\right) + \frac{\partial}{\partial y}\left(\frac{U_j V_j}{H_j}\right) - fV_j = -gH_j\frac{\partial \Phi_j}{\partial x} + \mathrm{AH}_j\nabla^2\left(\frac{U_j}{H_j}\right) - A_4 H_j \nabla^4\left(\frac{U_j}{H_j}\right) + \frac{\tau^x}{\rho_j}\delta_{1_j}. \tag{2}$$

Similarly, for the meridional transport V_j we have

$$\frac{\partial V_j}{\partial t} + \frac{\partial}{\partial x}\left(\frac{U_j V_j}{H_j}\right) + \frac{\partial}{\partial y}\left(\frac{V_j^2}{H_j}\right) + fU_j = -gH_j\frac{\partial \Phi_j}{\partial y} + \mathrm{AH}_j\nabla^2\left(\frac{V_j}{H_j}\right) - A_4 H_j \nabla^4\left(\frac{V_j}{H_j}\right) + \frac{\tau^y}{\rho_j}\delta_{1_j}. \tag{3}$$

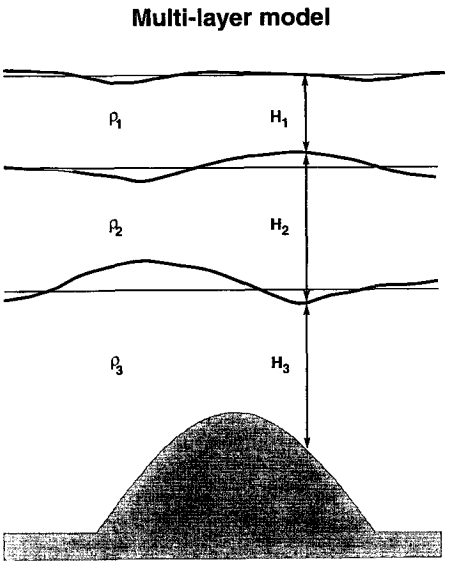

FIG. 1. Vertical structure of the isopycnal layered model.

In the equations above, g is the acceleration of gravity, while τ is the wind stress. We adopt the β-plane approximation, that is, the Coriolis parameter is $f = f_0 + \beta y$. The horizontal friction coefficients are A for harmonic friction and A_4 for biharmonic friction. The vertically integrated pressure anomaly is found using the hydrostatic approximation. We define a dynamic height as the vertically integrated pressure divided by $g\rho_j$:

$$\Phi_j = \eta - \sum_{i=1}^{j-1} \frac{(\rho_j - \rho_i)}{\rho_j}(H_i - H_{0i}), \tag{4}$$

where the depth H_{0i} is the layer thickness for an ocean at rest, and the Boussinesq approximation, that is, $\eta\rho_1/\rho_j = \eta$, has been applied. With N layers the surface displacement η is given by

$$\eta = \sum_{i=1}^{N} (H_i - H_{0i}). \tag{5}$$

The continuity equation becomes

$$\frac{\partial H_j}{\partial t} + \left(\frac{\partial U_j}{\partial x} + \frac{\partial V_j}{\partial y}\right) = A_H \nabla^2 H_j, \tag{6}$$

where it has been assumed that there is no mass exchange between the layers and isopycnal thickness mixing (Gent and McWilliams 1990) with a constant diffusion coefficient A_H may be applied for non-eddy-resolving applications.

Equations (2), (3), and (6) above are solved using a leapfrog time integration scheme and centered-in-space finite differences. The only exception is the diffusion term, where an Euler forward scheme is used. That term is computed at the oldest available time level, which results in a time step twice as long as the leapfrog

step. The pressure and the surface elevation are calculated from the diagnostic Eqs. (4) and (5). Discretization is on a C grid [see Arakawa and Lamb (1977) for a discussion of the properties]. The use of a fully explicit scheme severely restricts the time step since the fast barotropic mode is included. An alternative to the implicit methods and time-splitting methods mentioned in the introduction, a simple way to slow down these fast modes, is explored in the next section.

3. Method

For compressible fluids, the continuity equation is

$$\frac{1}{\gamma_*}\frac{\partial p}{\partial t} = -\nabla\cdot\mathbf{u}, \tag{7}$$

where $1/\gamma_*$ is the compressibility and $\gamma_* = \rho c_s^2$, where c_s is the speed of sound. In the method of artificial compressibility (Chorin 1967), an artificially reduced value of c_s is used to slow down the propagation of sound waves. The method is actually applied to solve incompressible flow problems, where the speed of sound equals infinity, but where sound waves inherently are unimportant for the solution.

If we integrate the time discretized version of (6) vertically, we obtain by use of (5)

$$\frac{\eta^{n+1} - \eta^{n-1}}{2\Delta t} = -\gamma \sum_{i=1}^{N}\left(\frac{\partial U_i^n}{\partial x} + \frac{\partial V_i^n}{\partial y}\right), \tag{8}$$

where n refers to the time level and a factor γ has been included in analogy with (7). The similarity of (7) and (8) suggests that we can reduce the phase speed of the external gravity waves by choosing the nondimensional parameter $\gamma \leqslant 1$. Hunter (1990a,b) implemented the method for a homogeneous fluid by solving Eq. (8) for a single layer. However, in this case, since (8) is not solved, the method is introduced by rewriting (4) as

$$\Phi_j = \gamma\eta - \sum_{i=1}^{j-1}\frac{(\rho_j - \rho_i)}{\rho_j}(H_i - H_{0i}). \tag{9}$$

Note that only the part of the pressure related to the surface deviation is modified. In contrast, the method by Bryan (1984), works by dividing the momentum equations (except the time derivatives) by a constant $\alpha \gg 1$. Since both the pressure gradient term and the Coriolis term are modified, the phase speed of Rossby waves is strongly affected, except the longest waves (see Fig. 1 in his paper). Since α is a global constant that stretches time, all vertical levels are modified. Consequently, baroclinic and barotropic modes are affected in the same way. In the following sections we will find that this is not the case with the method used here.

a. Wave properties

The method will be analyzed using the linear equations without friction. For simplicity we assume that there are no gradients in the y direction. The equations are

$$\frac{\partial U_j}{\partial t} - fV_j = -gH_{0j}\frac{\partial \Phi_j}{\partial x} \tag{10}$$

and

$$\frac{\partial V_j}{\partial t} + fU_j = 0, \tag{11}$$

where Φ_j is given by (9) and η by (5).

The continuity equation becomes

$$\frac{\partial H_j}{\partial t} = -\frac{\partial U_j}{\partial x}. \tag{12}$$

Taking $\partial/\partial t$ of (10), using (11) to eliminate V_j and (12) to eliminate H_j in (9) and (5), we obtain

$$\left(\frac{\partial^2}{\partial t^2} + f^2\right)U_j = g\mathbf{A}\frac{\partial^2 U_i}{\partial x^2}, \tag{13}$$

where the matrix $\mathbf{A}$ has the elements given by

$$a_{ji} = \left[\gamma - \frac{\rho_j - \rho_{\min(j,i)}}{\rho_j}\right]H_{0j}. \tag{14}$$

The N eigenvalues, $h^{(n)}$, $n = 0, \cdots, N-1$, of the matrix a_{ji} are the equivalent depths for the gravity waves. Hence, the dispersion relation is

$$\omega^2 - f^2 - gh^{(n)}k^2 = 0 \tag{15}$$

for the mode n Poincaré wave. The phase speed of the gravity wave is calculated from (15) as $c = \omega/k$.

b. Gravity waves in a two-layer model

For two layers we can easily find the eigenvalues of the matrix

$$\mathbf{A} = \begin{bmatrix} \gamma H_{01} & \gamma H_{01} \\ (\gamma - \Delta\rho/\rho)H_{02} & \gamma H_{02} \end{bmatrix}, \tag{16}$$

where the notation $\Delta\rho = \rho_2 - \rho_1$ and $\rho = \rho_2$ have been introduced. The eigenvalues are then given by

$$h^{(0,1)} = \frac{1}{2}\gamma H \pm \frac{1}{2}\gamma H\left(1 - \frac{4\Delta\rho H_{01}H_{02}}{\rho\gamma H^2}\right)^{1/2}, \tag{17}$$

where $H = H_{01} + H_{02}$. Since $H_{01}H_{02} < H^2/4$, the last term under the root is less than $\Delta\rho/\gamma\rho$. If this last term is much less than 1, we simply obtain the eigenvalues

$$h^{(0)} = \gamma H; \quad h^{(1)} = \frac{\Delta\rho H_{01}H_{02}}{\rho H}, \tag{18}$$

which is the approximation for the eigenvalues given in the literature for a linear two-layer model (e.g., Gill 1982, 121–122). Note that the internal mode to a first approximation is independent of γ, while the equiva-

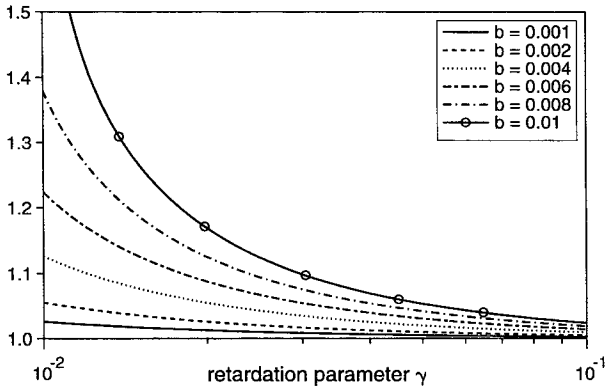

FIG. 2. Ratio R_h of modified to exact equivalent depth (or phase speed squared) for the internal gravity wave in a two-layer ocean as a function of the retardation parameter γ. Curves are shown for a range of values of the parameter b defined in the text.

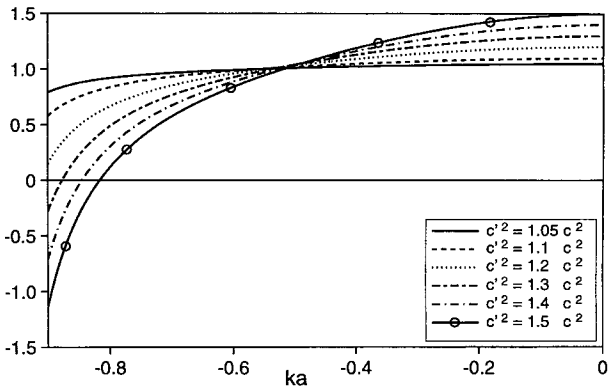

FIG. 4. As in Fig. 3 but for the group velocity of long baroclinic Rossby waves.

lent depth for the external mode has been decreased by a factor γ. The technique can therefore be referred to as a gravity wave retardation (GWR) method for the external mode, where γ is the retardation parameter.

If we write $H_{01} = \alpha H$ and $H_{02} = (1 - \alpha)H$, and use (17), the ratio of $h^{(0,1)}$ to the exact equivalent depth is

$$R_h = \frac{\gamma \pm (\gamma^2 - \gamma b)^{1/2}}{1 \pm (1 - b)^{1/2}}, \qquad (19)$$

where the parameter $b = 4\alpha(1 - \alpha)\Delta\rho/\rho$ has a maximum of $\Delta\rho/\rho$ for $\alpha = 1/2$. In all realistic cases the stratification is weak, that is, $b \ll 1$ and Eq. (19) requires that $b \leqslant \gamma$ for real solutions. Assuming those two conditions, and $b = \epsilon\gamma$ with $\epsilon \leqslant 1$, we find that $1 \leqslant R_h \leqslant 2$. As the wave retardation parameter γ is decreased for a given $b \ll 1$, for example, as $\gamma \to b$, $R_h \to 2$ for the internal mode. This means that the phase speed of the internal gravity waves is increased by a factor $\sqrt{2}$ and that the external wave speed approaches the internal wave speed. Figure 2 shows the ratio R_h as a function of γ for various values of the parameter b. Typical, for basin-scale applications, b will be about 10^{-3} or less. This corresponds to only a few percents error on the phase speed. For the reduced gravity model, where one assumes the lowest layer is infinitely deep, the ratio corresponding to R_h equals $(H_1 + H_2)H_2^{-1}$. This error will typically be of the same order or larger than the phase error made using gravity wave retardation.

c. Rossby waves

For the system of equations, modified by γ, we get the usual dispersion relation for Rossby waves

$$\omega = -\beta k\left(k^2 + l^2 + \frac{f_0^2}{c'^2}\right)^{-1}, \qquad (20)$$

where (k, l) are the wavenumbers in the x and y directions, f_0 the Coriolis parameter, and c' the modified gravity wave speed. Errors in the gravity wave speed

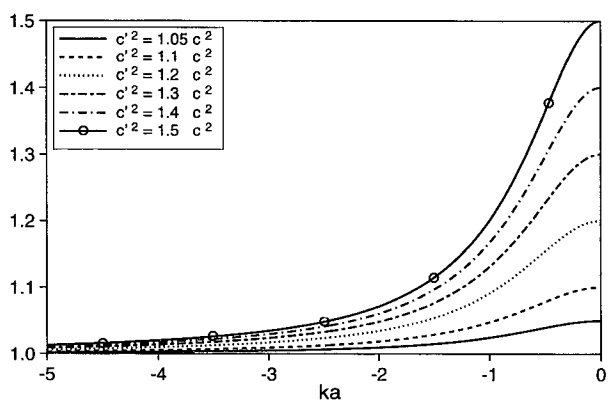

FIG. 3. Ratio of modified phase speed to exact phase speed for baroclinic Rossby waves as function of ka, which is the wavenumber k multiplied by the exact Rossby radius of deformation a. Curves are shown for a range of values of modified internal gravity wave speeds c'^2.

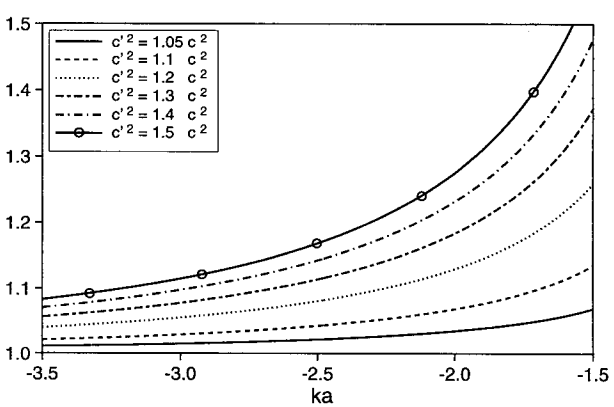

FIG. 5. As in Fig. 3 but for the group velocity of short baroclinic Rossby waves.

will mostly influence long waves. Figure 3 shows the relative phase speed of modified baroclinic Rossby waves to the exact theoretical speed with $\gamma = 1$. The error is less than that for the gravity waves. However, the group velocity is more sensitive to changes in gravity wave speed. Waves with $|1/k|$ smaller than the Rossby deformation radius a or larger than about $2a$, have increased energy propagation speed (Figs. 4 and 5). In the vicinity of $ka = 1$, the group velocity vanishes, which obviously results in large relative errors.

Barotropic Rossby waves are slowed down when the barotropic gravity wave speed is reduced. Figures 6 and 7 show the phase speed and group velocity, respectively, relative to the correct speeds. Fortunately, barotropic waves are short waves compared to the barotropic deformation radius (about 2000 km). Typically, ka is about 20 or larger, corresponding to wavelength shorter than $a/3$. However, the reduction of the group velocity is significant. For instance, if c^2 is reduced by a factor 100, a wave with $ka = 20$, will have an 50% error for propagation of energy. This implies that the barotropic adjustment to changes in wind stress curl will be too slow. However, it will still be much faster than the baroclinic response, so in case of spinup of the ocean toward a quasi-steady state, this should not cause serious problems as the results shown in section 4c suggest.

d. Steady flows

The simple case of steady response for a two-layer model to a constant wind stress is a balance between pressure gradient and wind stress in the case of no rotation. Neglecting other frictional forces than the wind stress, the linearized solution to Eqs. (2)–(4) is

$$\frac{\partial H_1}{\partial x} = \frac{\tau^x \rho_2}{g \rho_1 H_{01} (\rho_2 - \rho_1)} \tag{21}$$

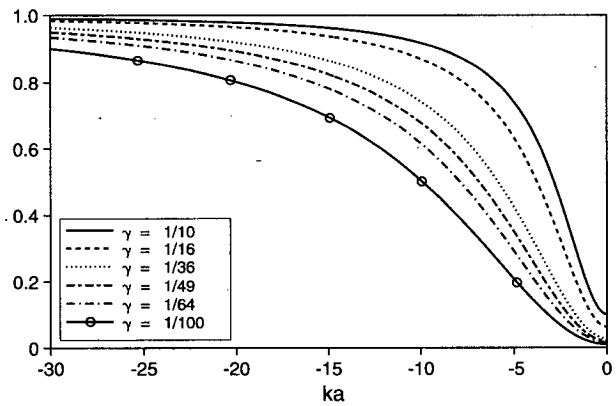

FIG. 6. As in Fig. 3 but for the phase speed of barotropic Rossby waves.

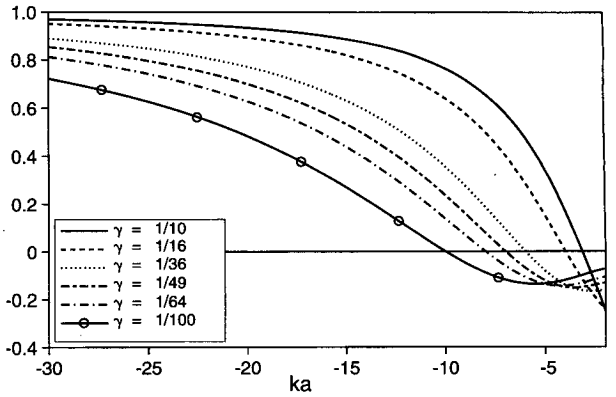

FIG. 7. As in Fig. 3 but for the group velocity of short barotropic Rossby waves.

and

$$\frac{\partial H_2}{\partial x} = \left(\frac{\rho_2 - \rho_1}{\gamma \rho_2} - 1 \right) \frac{\tau^x \rho_2}{g \rho_1 H_{01} (\rho_2 - \rho_1)}, \tag{22}$$

where $H_{0j}, j = 1, 2$ indicates the initial condition. Note that the upper-layer thickness gradient does not depend on γ, while the compensating gradient of the lower-layer thickness is reduced in magnitude. Also note that the surface elevation gradient, which is the sum of Eqs. (21) and (22), is increased by a factor $1/\gamma$. This leaves the pressure gradient unchanged for both layers. Since the model surface elevation is artificially amplified, Hearn and Hunter (1987) suggested that it should be reduced by a factor γ when compared to observations.

For flows where the Coriolis force f is important, the length scale for adjustment is the Rossby radius of deformation, c/f where c is the gravity wave speed. It is obvious that this scale is dramatically reduced for the barotropic component. We can therefore expect order one errors for the barotropic component in boundary currents and jets. Fortunately, the major western boundary currents, such as the Gulf Stream, are mainly baroclinic.

e. Relation to reduced-gravity layer models

For multilayer reduced gravity layer models, the deepest layer, N, is assumed infinitely deep, which removes the barotropic mode entirely. In that case the dynamic height is given by

$$\Phi_j = \sum_{i=1}^{N-1} \frac{(\rho_N - \rho_i)}{\rho_N} (H_i - H_{0i}) - \sum_{i=1}^{j-1} \frac{(\rho_j - \rho_i)}{\rho_j} (H_i - H_{0i}) \tag{23}$$

(Jensen 1991). The relative density difference between the upper ocean and the deep ocean, $\Delta\rho/\rho$ is typically 3×10^{-3}. This suggests that we can choose values of

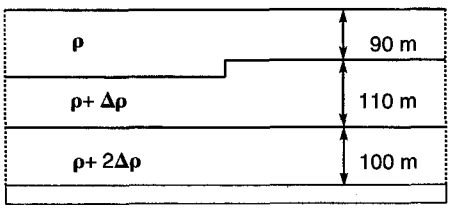

FIG. 8. Vertical cross section of the initial condition for internal wave propagation test.

γ down to that value, if we are not interested in the barotropic mode.

4. Examples of applications

a. Internal gravity waves

First we consider an infinitely long channel with flat bottom. It is assumed that there are no variations in one of the horizontal directions, and that there is no rotation ($f = 0$). A harmonic diffusion coefficient of 50 $m^2\ s^{-1}$ for momentum was applied and the grid spacing was 11 km. The channel has three layers, each 100 m thick on average, making the total depth 300 m. The density jump between the layers is constant (1.55×10^{-3} kg m^{-3}). This depth and stratification results in a long surface gravity wave speed of 54 m s^{-1}, and internal gravity wave modes with phase speeds of 1.215 m s^{-1} and 0.702 m s^{-1}. Selecting $\gamma = 1/64$, the wave speeds are modified to be 6.618, 1.246, and 0.700 m s^{-1}. The first baroclinic mode can consequently be expected to propagate with a speed that is 2.6% too fast.

In this experiment there is no external forcing. The initial condition (Fig. 8) is a steplike change of 20 m in upper-layer thickness, compensated by the thickness of layer 2, so that layer 3 is unperturbed. The surface is level, which means that there are no pressure gradients in layer 1 at the onset. In layer 2 and 3 there is a horizontal pressure discontinuity (high pressure to the right in Fig. 8), which accelerates the flow in the direction of low pressure.

The external gravity wave elevates the surface to the left (caused by flow toward low pressure in layers 2 and 3) and lowers it to the right. This surface front moves away from the discontinuity with the fast external gravity wave speed.

Away from the initial discontinuity, the thickness of layer 2 is nearly constant until the front associated with the 2 vertical mode passes. This is because flow in layer 3 compensates the transport in layer 1. A projection of the solution on vertical modes (see Lighthill 1969) also reveals a very small amplitude of the 1 vertical mode in layer 2.

After passage of the fronts, the final stage is a flow from left to right in the top layer, with weaker flows in the opposite direction in the two lower layers. Since there is no rotation, all available potential energy has been converted into kinetic energy. For similar examples see Gill (1982, 110 and 164).

Figures 9a,b show the thickness of layer 1 and the associated currents in a x–t diagram for $\gamma = 1$ (we will refer to that as the standard case) and $\gamma = 1/64$. It is seen that the solutions are very close, with a slight increase (3%) in the 1 baroclinic wave speed and no difference in the 2 baroclinic wave speed, as predicted by linear theory. Note that no currents appear for a while in Fig. 9b. This is because the external gravity wave has been slowed down. For the standard case, the external wave propagates out of the area in less than 2 h, which is too fast to be visible in Fig. 9a, so it appears as if very weak currents (appearing only as dots in Fig. 9a) exist at $t = 0$.

While the correct surface elevation is less than 0.02 m, the case with reduced wave speed have deviations up to 0.9 m. This results in an error for the barotropic mode of about 0.01 m s^{-1}, while the magnitude of total velocity is 0.1 m s^{-1}. However, the propagation of the baroclinic waves and the baroclinic currents are well represented.

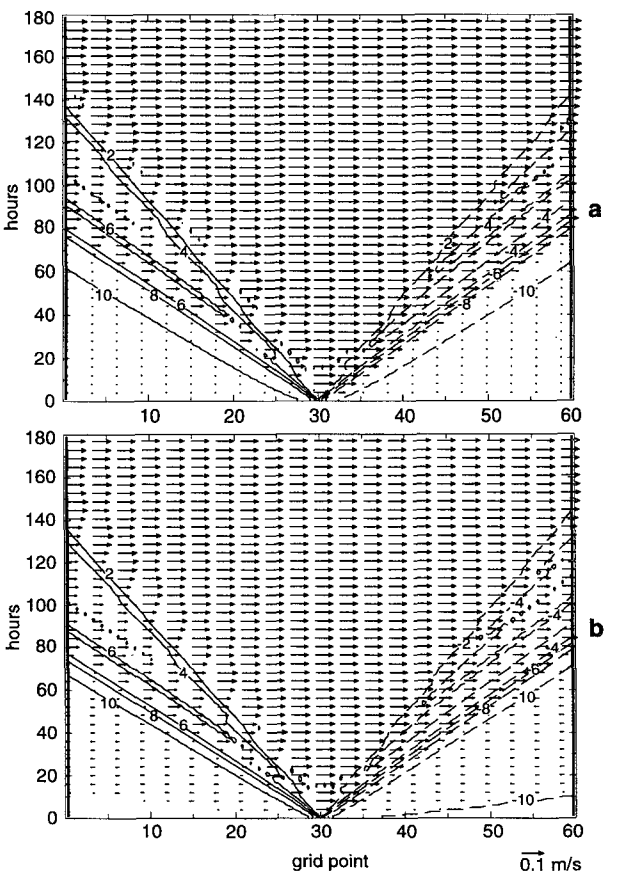

FIG. 9. Time evolution of upper-layer thickness anomaly and velocity vectors along the central 660 km of the basin. The slope of the fronts give the phase speed of the vertical modes. (a) Standard case ($\gamma = 1$). (b) GWR case ($\gamma = 1/64$).

b. Response to zonal equatorial wind

In the tropical ocean the barotropic mode is less important than in midlatitudes. The equatorial response of the Yoshida jet (Yoshida 1959; Gill 1982, p. 459) is therefore considered next. An equatorial β-plane ocean is used with dimensions 7150 km (east–west) and 4400 km (north–south). This corresponds to 65° in longitude at the equator and from 20°S to 20°N in latitude. Periodic boundary conditions are used in the east–west direction, while walls limits the ocean at the southern and northern boundaries. The horizontal resolution is 55 km, a harmonic diffusion coefficient for momentum of 500 $m^2\ s^{-1}$ was applied, and three layers of 100-, 100-, and 2000-m depth were used. The density jump across each layer is the same as in the previous example. This results in gravity wave speeds of 147, 1.88, and 0.749 $m\ s^{-1}$. After applying a steady, spatial uniform wind stress (0.1 $N\ m^{-2}$) for 10 days the jet is well developed. For $\gamma = 1/256$, the maximum error in the zonal baroclinic velocity field is only 0.25% in layer 1 and up to 3% in layer 3. The largest error appears in the lower-layer thickness anomaly, which is reduced as discussed in section 3d. Instead of a positive anomaly of about 4 m, the anomaly goes to zero for decreasing $\gamma = 1/256$ (Fig. 10). The barotropic solution is an equatorial jet trapped within a few equatorial Rossby deformation radii $(c/\beta)^{1/2}$ where c is the gravity wave speed. Outside the region defined by the deformation radius, based on the retarded wave speed, we can expect large relative errors, since the baroclinic currents are weak for this test case. Within that region, the baroclinic flow is strong, and relative errors will be small. As shown in Fig. 11 the barotropic mode has a much reduced radius of deformation for $\gamma \ll 1$, and order one errors will obviously occur for this mode away from the equator. In particular, the divergence of the retarded flow is concentrated in a much smaller area than in the standard case. Associated with the divergence is a decrease in total fluid depth, mainly due to a reduced layer 3 thickness. The tendency for the barotropic flow is to cancel the baroclinic flow in layer 3 in the retarded wave case. This is to be expected, since layer 3 is much deeper than the two upper layers. For that layer structure, applying the GWR method as in Eq. (9) with $\gamma \ll 1$, corresponds essentially to using a reduced gravity layer model, that is, Eq. (23).

A dynamically similar situation occurs when a coastal jet is forced with an alongshore wind that decays offshore. Large errors appear in the barotropic flow only offshore, outside the region where the baroclinic part of the coastal jet dominates. However, in shallow coastal areas, the surface elevation error (several meters) becomes relatively large and introduces additional errors.

c. Spinup of midlatitude ocean

For climate modeling it is a key point whether the quasi-steady, large-scale circulation is modeled fairly accurately. We consider a rectangular ocean, which spans 4763 km in the zonal direction and 4400 km in the meridional direction (10°–50°N). The β-plane approximation, centered on 30°N, is used. The horizontal resolution is 47.6 km in the zonal direction and 55 km in the meridional direction. Three layers of 200 m, 200 m, and 1600 m thickness, respectively, were used. The time step ranged from 100 s (no retardation) to 1600 s ($\gamma = 1/256$). Harmonic and biharmonic diffusion were used in the momentum equations, with coefficients of 5000 $m^2\ s^{-1}$ and $2 \times 10^{13}\ m^4\ s^{-1}$, respectively. Isopycnal thickness diffusion, using a coefficient of 5000 $m^2\ s^{-1}$, was also applied. The relatively high values for diffusion enables the western boundary current to be resolved and limits the effects of nonlinear momentum advection, that is, by providing low–Reynolds number

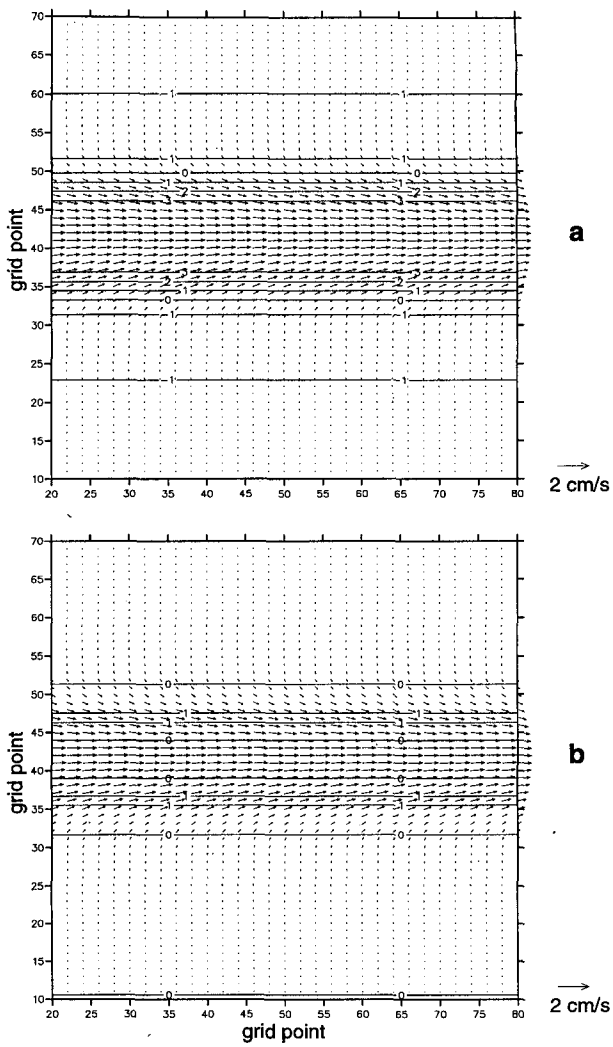

FIG. 10. Baroclinic part of the flow in layer 3 at day 10 with $\gamma = 1$ (a) and $\gamma = 1/256$ (b). Only a small difference in the contours of thickness anomaly for layer 3 is seen. Contour level interval is 1 m. Grid spacing is 55 km.

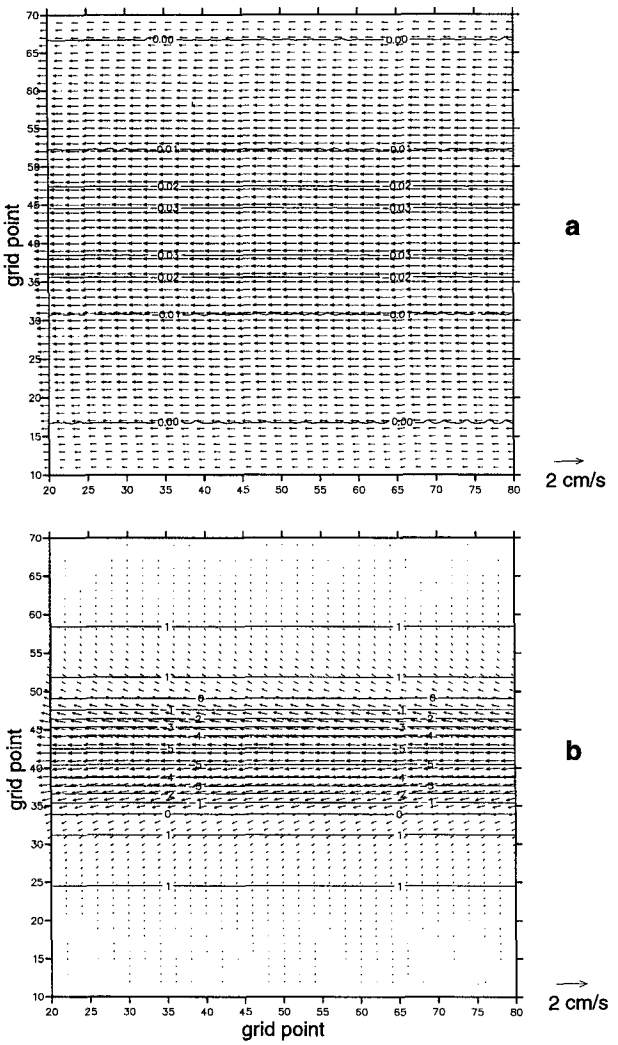

FIG. 11. The barotropic currents and surface deviation after 10 days. Without gravity wave retardation, the barotropic equatorial jet is wide (a). For a large reduction in external gravity wave speed (a factor of 16 is used here), the barotropic part of the jet is narrower due to the reduced Rossby radius of deformation (b). Contour level intervals for the surface deviation are 0.01 m (a) and 1 m (b).

solutions, which may be compared without any time averaging.

The ocean was spun up from rest with a zonal wind stress varying with latitude as

$$\tau^x = -0.1 \cos\left(\frac{\pi y}{L_y}\right) \quad (\mathrm{N\ m^{-2}}), \qquad (24)$$

where L_y is the north–south length of the basin, and y is measured from the southern edge. In addition, the wind stress is tapered linearly toward zero within a 550-km-wide zone along the northern and southern boundary (see Fig. 12). This is done in order to avoid upwelling and downwelling along the artificial northern and southern boundaries. The magnitude of the wind stress has been linearly increased from zero to the value given by Eq. (24) over 10 days and then held constant.

In the following, the depth-averaged currents are referred to as the barotropic part of the flow, although this is not exactly true as discussed in the introduction. Similarly, the total flow minus the depth-averaged flow will be referred to as the baroclinic part. The depth-averaged currents and surface displacement (multiplied by γ) after 360 days of integration are shown in Fig. 12 without retardation, with $\gamma = 1/64$, and with $\gamma = 1/256$. The effect of slowing down the gravity wave

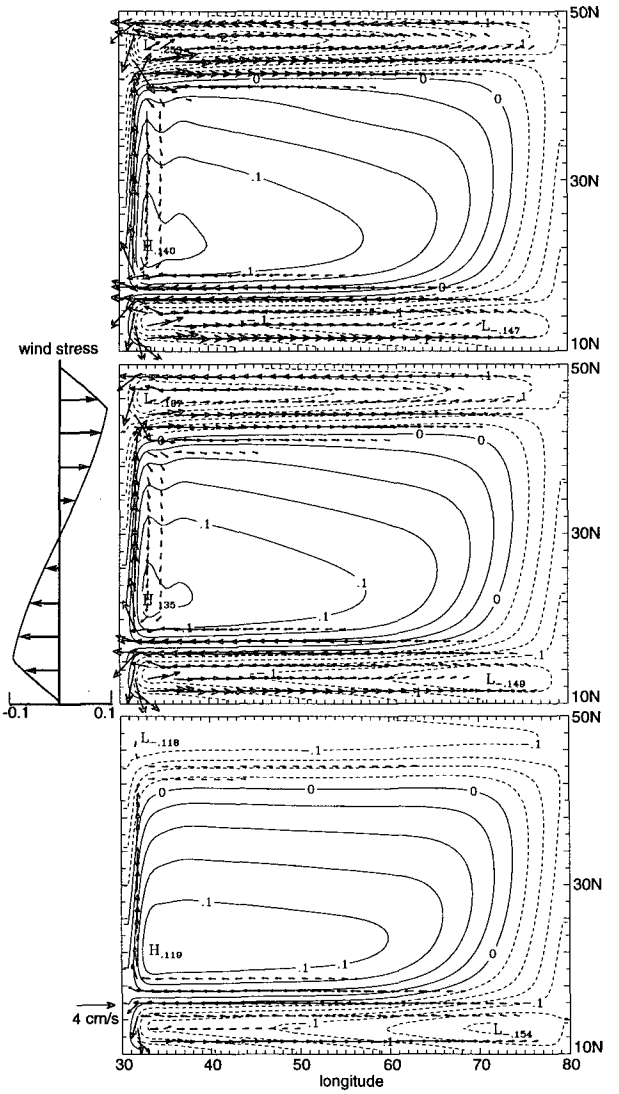

FIG. 12. Barotropic circulation of three-layer ocean with a flat bottom after 360 days of integration with $\gamma = 1$ (top), $\gamma = 1/64$ (center), and $\gamma = 1/256$ (bottom). Current vectors larger than 4.0 cm s^{-1} have been truncated. Contours show the total depth anomalies multiplied by γ (corresponding to a realistic surface deviation) in meters. Contour interval is 0.025 m.

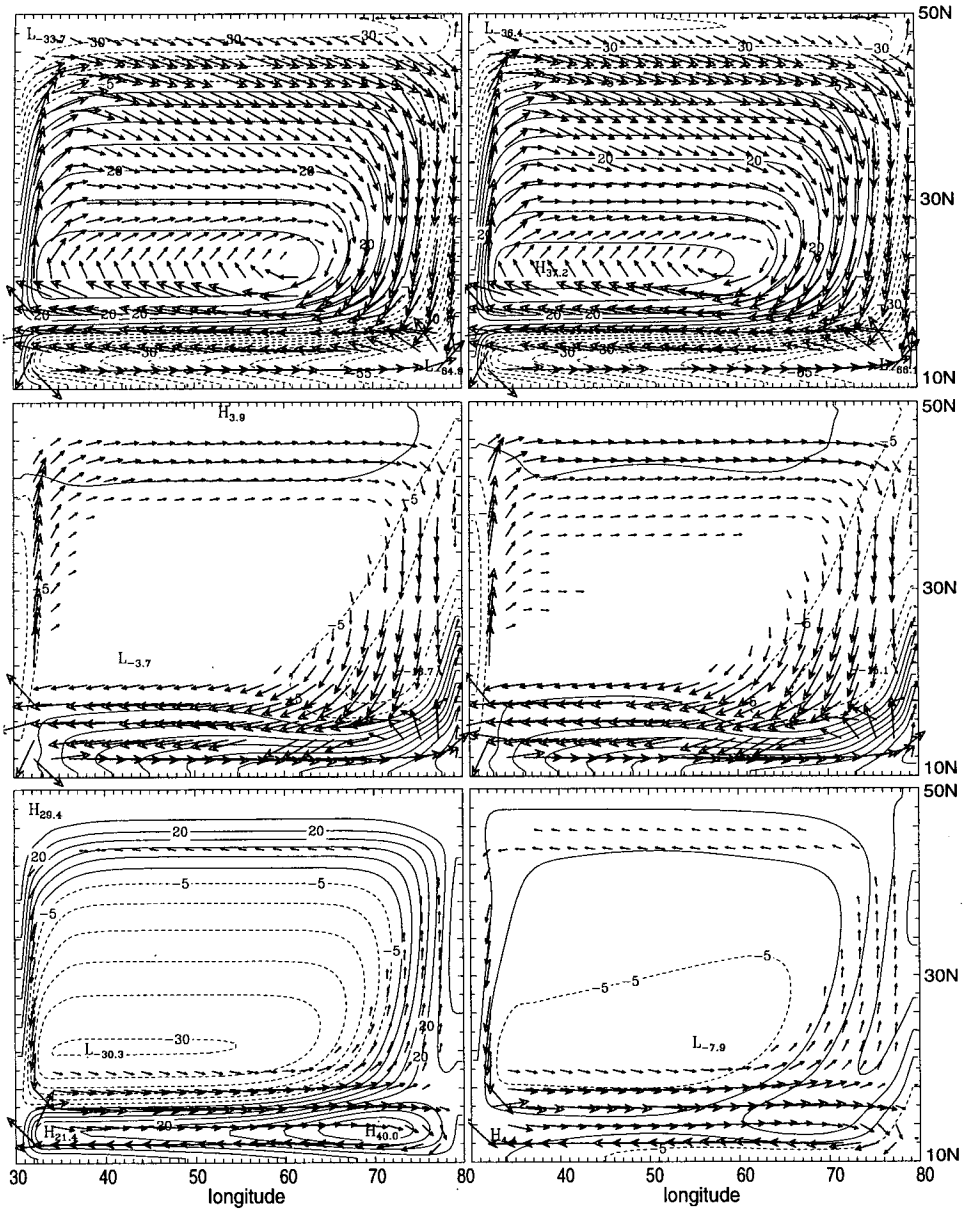

FIG. 13. Baroclinic circulation of three-layer ocean with flat bottom after 360 days of spinup. The flow in layers 1–3 is shown from top to bottom. Isolines show layer thickness anomalies for each layer with a 5-m contour interval. Results without gravity wave retardation (left) and with a reduction of the external gravity wave speed by a factor 16 (right). Current vectors larger than 1.0 cm s^{-1} have been truncated.

speed, and consequently the barotropic Rossby wave propagation (see Figs. 6 and 7), is to reduce the overall barotropic response. For $\gamma = 1/64$, the results are reasonable, with typical errors of about 20% or less in the barotropic current speed. For $\gamma = 1/256$, the barotropic currents are only about 40% of the correct magnitude. The actual amplitude of the model surface elevation anomalies increases with increased retardation. For $\gamma = 1/256$ and $\gamma = 1/64$, the maximum amplitude is about 40 and 10 m, respectively, compared to 25 cm for $\gamma = 1$. However, when multiplied by γ (Hearn and Hunter 1987), the surface elevations for the GWR cases compare fairly well with the standard case.

The baroclinic part of the currents are shown in Fig. 13 for the correct gravity wave speed (left) and for $\gamma = 1/256$. The baroclinic currents are typically slightly larger in magnitude for the case with gravity wave retardation (by about 10% for $\gamma = 1/256$). However, the results in Fig. 13 are remarkably similar given the factor of 16 in computer time between the two computa-

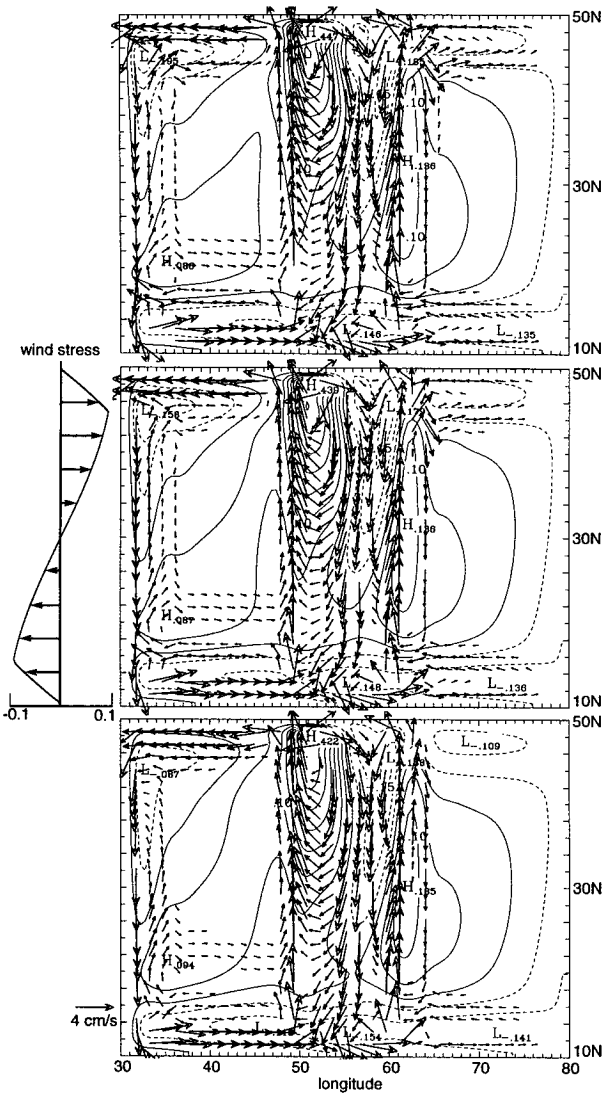

FIG. 14. As in Fig. 12 but for flow over ridge. Contour interval is 0.05 m.

tions. We note that the thickness anomaly for layer 3 is significantly reduced compared to the standard case. This is associated with the change in total depth as we observed in Fig. 12.

The model was also applied to the barotropic case with the same forcing. The errors were smaller than for the case with stratification, but the intensity of the circulation was also weakened with increasing retardation. As in Fig. 12, the error is largest in the north, where the adjustment time for the ocean is the longest.

d. Flow over midocean ridge

Given the encouraging results for a flat bottom, it would be interesting to see if the method would work as well when bottom topography was added. The case from the last section was repeated with a north–south aligned ridge in the center of the basin. The ridge varied as a cosine function (Fig. 1) with an amplitude of 800 m, which is half the thickness of the lower layer. The width of the depth anomaly was 24% of the width of the basin. Figure 14 shows the barotropic part of the flow ($\gamma = 1$, $1/64$, and $1/256$) and Fig. 15 the baroclinic part ($\gamma = 1$ and $1/256$). The ridge strongly modifies the flow in all three layers. There are essentially separate eastern and western circulation cells. The results are better than in the flat-bottom case, most likely due to a shorter spinup time for the reduced effective east–west length scale of the circulation. Over the ridge, we can in principle increase γ without violating the stability criterion. We tried to apply

$$\gamma = \min\left(\frac{\gamma_0 D_{\max}}{D}, 1\right), \tag{25}$$

where D is the depth of the ocean, $D_{\max}$ is the maximum depth, and γ_0 is the minimal γ used. However, the results were not as good as with a constant γ.

5. Discussion

By slowing down the gravity waves, we are distorting the dynamics and introducing errors, and one might question why an obviously less accurate method than using the exact gravity wave speed is of any practical use. Clearly, the objective is to save computer time. This is also why implicit methods are used, but they will also alter the solution of atmospheric and oceanic flows by slowing down wave propagation, if Courant numbers much larger than one are used (Grotjahn and O'Brien 1976).

The method of artificially reducing the propagation of external modes is useful for modeling oceanic flows where the baroclinic modes dominate. For such flows, the phase speed may be reduced by a factor up to 10 or more without significant errors. As shown in section 4, the baroclinic part of the flow was modeled remarkably well for very small values of γ. The method does slow down barotropic Rossby waves, energy propagation in particular, so when the dynamics of these waves are important, the phase speed of the external gravity waves should only be decreased by a factor 4–5. To emphasize the differences between the reference solution and the GWR solution, we selected smaller values of γ, than should be applied for applications where the barotropic mode is of any interest.

The GWR method can be applied to spin up the ocean for decadal simulations of seasonal forced oceanic flow. In the last few years of the simulation, the external gravity wave speed can be gradually increased to minimize errors in the final seasonal circulation. The method of Bryan (1984) is without question much better suited for centuries of spinup of an ocean subject to steady forcing. For time-dependent flow, short baro-

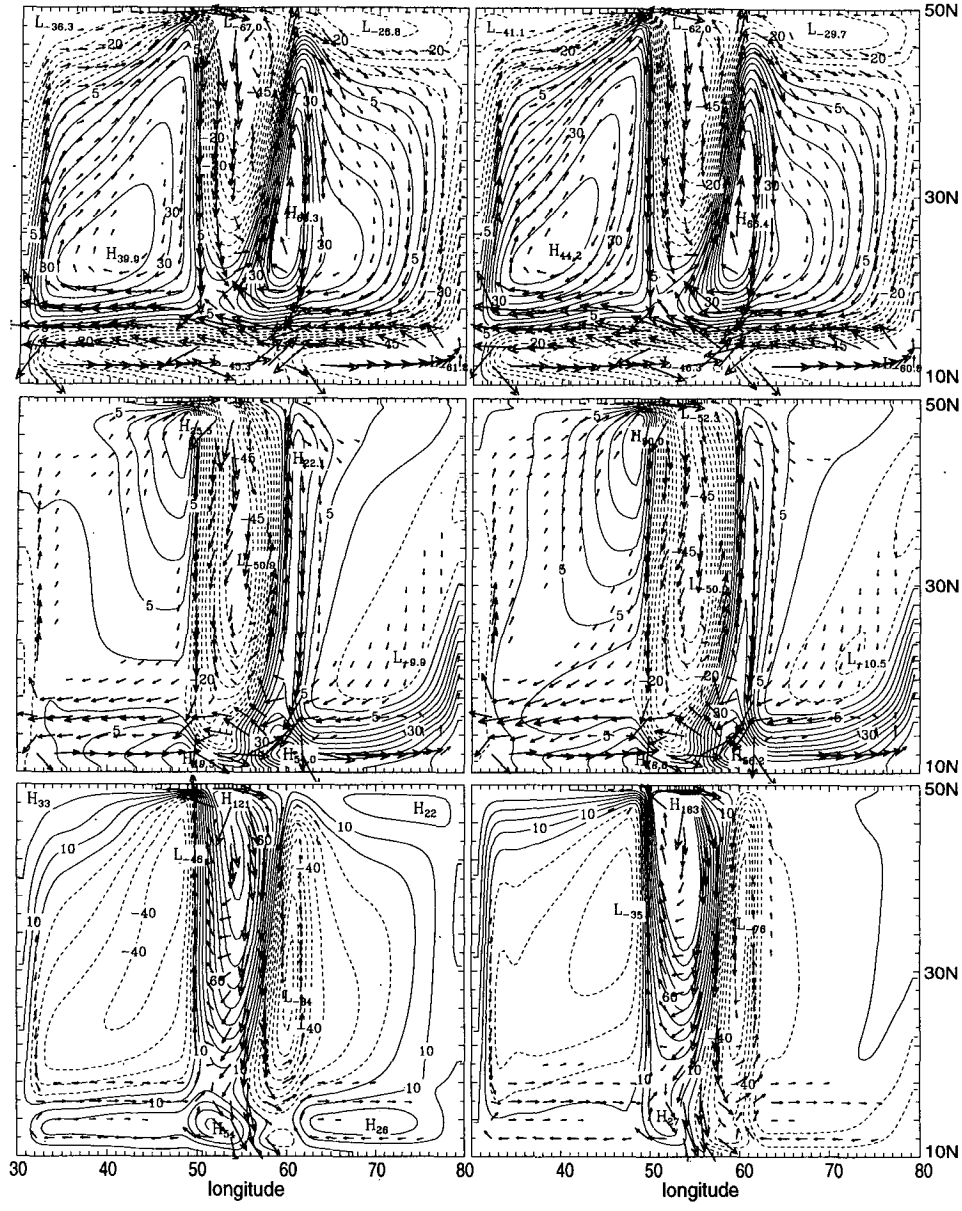

FIG. 15. As in Fig. 13 but for flow over ridge. Contour intervals are 5 m (two upper panels) and 10 m (layer 3, bottom panel). Only contours up to 100 m are shown. Current vectors larger than 4.0 cm s^{-1} have been truncated.

clinic Rossby waves are important and can be more accurately modeled using the method presented here.

The impact of using retardation methods on the oceanic heat transport still needs to be investigated. The thickness anomaly of the lower layer is significantly reduced when a very small value of the retardation parameter γ is used. This may result in errors in the heat transport in the deep ocean. Because of the error in lower-layer thickness, an error of the same order of magnitude occurs in the total ocean depth and consequently for the surface elevation. To compare model surface elevations with observations, the model results must be multiplied with the retardation parameter. The surface elevation results shown here are encouraging, but if the barotropic radius of deformation is reduced by a large factor, one cannot always expect to find good correlations between model and observations.

The GWR method can also be used for preliminary investigations, where very accurate solutions may not be needed. This makes it possible to simulate a large number of flow scenarios, which otherwise would be prohibitive due to computational costs. Most impor-

tantly, the method can be seen as a more general alternative to multilayer reduced gravity layer models, which, in spite of the lack of the barotropic mode and bottom topography, have been quite successfully used for ocean modeling.

Acknowledgments. The idea of using a reduced value of gravity for surface waves was suggested to me by John Anderson, University of Wisconsin at a CHAMMP Science Team Meeting, March 1993. Most computations were done on the CRAYs at NERSC, Lawrence Livermore National Laboratory. This research was supported by DOE CHAMMP program, Grant DE-FG02-92ER61440 to Colorado State University and by the Danish National Research Foundation (Dansk Grundforskningsfond), which funds the International Research Centre for Computational Hydrodynamics (ICCH).

REFERENCES

Arakawa, A., and V. R. Lamb, 1977: Computational design of the basic dynamical processes of the UCLA general circulation model. Vol. 17, *Methods in Computational Physics,* J. Chang, Ed., Academic Press, 173–265.

Bleck, R., and L. Smith, 1990: A wind-driven isopycnic coordinate model of the North and equatorial Atlantic Ocean. Part I: Model development and supporting experiments. *J. Geophys. Res.,* **95,** 3273–3286.

Blumberg, A. F., and G. L. Mellor, 1987: A description of a three-dimensional coastal ocean circulation model. *Three-dimensional Coastal Ocean Models,* N. Heaps, Ed., Amer. Geophys. Union, 1–16.

Bryan, K., 1969: A numerical method for the study of the circulation of the World Ocean. *J. Comput. Phys.,* **4,** 347–376.

——, 1984: Accelerating the convergence to equilibrium of ocean–climate models. *J. Phys. Oceanogr.,* **14,** 666–673.

Chorin, A. J., 1967: A numerical method for solving incompressible viscous flow problems. *J. Comput. Phys.,* **2,** 12–26.

Cushman-Roisin, B., and J. J. O'Brien, 1983: The influence of bottom topography on baroclinic transports. *J. Phys. Oceanogr.,* **13,** 1600–1611.

Dukowicz, J. K., and R. D. Smith, 1994: Implicit free-surface method for the Bryan–Cox–Semtner ocean model. *J. Geophys. Res.,* **99,** 7991–8014.

Gent, P. R., and J. C. McWilliams, 1990: Isopycnal mixing in ocean circulation models. *J. Phys. Oceanogr.,* **20,** 150–155.

Gill, A. E., 1982: *Atmosphere–Oceans Dynamics.* Academic Press, 662 pp.

Grotjahn, R., and J. J. O'Brien, 1976: Some inaccuracies in finite differencing hyperbolic equations. *Mon. Wea. Rev.,* **104,** 180–194.

Hearn, C. J., and J. R. Hunter, 1987: Modelling wind-driven flow in shallow water systems on the southwest Australian coast. *Numerical Modelling: Applications to Marine Systems,* J. Noye, Ed., Elsevier, 47–57.

Hunter, J. R., 1990a: User manual for numerical hydrodynamic models of marine systems and associated plotting package. CSIRO Division of Oceanography, Rep. OMR-14/00, 73 pp.

——, 1990b: User manual for three-dimensional numerical hydrodynamic and dispersion model. CSIRO Division of Oceanography, Rep. OMR-24/00, 44 pp.

Jensen, T. G., 1991: Modeling the seasonal undercurrents in the Somali Current System. *J. Geophys. Res.,* **96,** 22 151–22 167.

——, 1993: Equatorial variability and resonance in a wind-driven Indian Ocean Model. *J. Geophys. Res.,* **98,** 22 533–22 552.

Killworth, P. D., D. Stainforth, D. J. Webb, and S. M. Paterson, 1991: The development of a free-surface Bryan–Cox–Semtner ocean model. *J. Phys. Oceanogr.,* **21,** 1333–1348.

Lighthill, M. J., 1969: Dynamic response of the Indian Ocean to onset of the southwest monsoon. *Philos. Trans. Roy. Soc. London, Ser. A,* **265,** 45–92.

Oberhuber, J. M., 1993: Simulation of the Atlantic circulation with a coupled sea ice-mixed layer-isopycnal general circulation model. Part I: Model description. *J. Phys. Oceanogr.,* **23,** 808–829.

Smith, R. D., J. K. Dukowicz, and R. C. Malone, 1992: Parallel ocean general circulation modeling. *Physica D,* **60,** 38–61.

Tobis, M., 1996: Effects of slowed barotropic dynamics in parallel ocean climate models. Ph.D. dissertation, University of Wisconsin—Madison, 198 pp.

Wallcraft, A. J., 1991: The Navy Layered Ocean Model Users Guide. Rep. 235, Naval Research Laboratory, Stennis Space Center, 21 pp.

Yoshida, K., 1959: A theory of the Cromwell Current and of equatorial upwelling. *J. Oceanogr. Soc. Japan,* **15,** 154–170.

Zhang, R.-H., and M. Endoh, 1992: A free surface general circulation model for the tropical Pacific Ocean. *J. Geophys. Res.,* **97,** 11 237–11 255.